Chapter 3
Transport Properties of Cubic Cuprous Iodide Films Deposited by Successive Ionic Layer Adsorption and Reaction

N. P. Klochko, K. S. Klepikova, D. O. Zhadan, V. R. Kopach, Y. R. Kostyuchenko, I. V. Khrypunova, V. M. Lyubov, M. V. Kirichenko, A. L. Khrypunova, S. I. Petrushenko and S. V. Dukarov

Abstract In this work we investigate crystal structure, morphology, and composition of CuI films produced in different modes of SILAR on glass plates and on flexible poly(ethylene terephthalate) (PET) substrates in connection with their transport properties, and with electrical and thermoelectric properties as a whole. Temperature dependences of resistivity for most CuI films have the crossover from semiconducting to metallic behavior with increasing temperature. The semiconductor carrier transport occurs in CuI films through nearest neighboring hopping. Metallic transport in CuI films carried out in accordance with the ionized impurity scattering and the carrier–carrier scattering model.

3.1 Introduction

Since an idea of invisible circuits conceived, transparent semiconductor devices have gained remarkable interest over the last years [1–8]. Another functionality added if taking into account transparent thermoelectric devices for power generation working at near room temperatures. Cubic cuprous iodide (γ-CuI, hereinafter CuI) is a promising intrinsically *p*-type conducting material both for transparent optoelectronics due to its high band gap of ≈3 eV at room temperature [1–7], and for thermoelectrics [1, 3, 6, 7]. To this day CuI is by far the best transparent *p*-type thermoelectric material with a room-temperature thermoelectric figure of merit of $ZT \approx 0.21$ [1]. As described in [1–7], CuI thin films are heavily doped and disordered degenerate semiconductors possessing properties of *p*-type transparent conductors. For example, a

N. P. Klochko (✉) · K. S. Klepikova · D. O. Zhadan · V. R. Kopach · Y. R. Kostyuchenko · I. V. Khrypunova · V. M. Lyubov · M. V. Kirichenko · A. L. Khrypunova
Materials Engineering for Solar Cells Department (MESC), National Technical University "Kharkiv Polytechnic Institute" (NTU "KhPI"), Kharkiv, Ukraine
e-mail: klochko.np16@gmail.com

S. I. Petrushenko · S. V. Dukarov
School of Physics, V. N. Karazin Kharkiv National University, Kharkiv, Ukraine

A. D. Pogrebnjak and O. Bondar (eds.), *Microstructure and Properties of Micro- and Nanoscale Materials, Films, and Coatings (NAP 2019)*,
Springer Proceedings in Physics 240, https://doi.org/10.1007/978-981-15-1742-6_3

record low room-temperature resistivity $\rho \approx 6.4 \times 10^{-5}$ Ω m has been shown in [6] for as-deposited and $\rho \approx 3.5 \times 10^{-5}$ Ω m for I-doped polycrystalline CuI thin films obtained in vacuum by reactive sputtering.

Moreover, thin films CuI are of particular interest for flexible wearable electronic and thermoelectric applications due to its unique properties and since they can be made on flexible substrates at near-room temperature. It is remarkable that CuI films suitable for barrier heterostructures [9] and for thermoelectric generators [10] can be synthesized from abundant resources using an inexpensive and suitable for large-scale production wet chemical Successive Ionic Layer Adsorption and Reaction (SILAR) method.

However, although CuI is the first discovered transparent conductive material, until now there are only a few publications regarding the analysis and understanding of its transport properties [1, 6, 7]. As can be seen from the temperature (T) dependence of the resistivity (ρ) reported in [1, 6, 7, 11], transport properties of the *p*-type CuI thin films are quite unusual. A crossover from semiconducting to metallic behavior with increasing temperature and a typical ρ minimum in the temperature-dependent resistivity graph has been shown in [1, 6, 11] for nanocrystalline CuI thin films obtained through different techniques, including vacuum evaporation [6] and SILAR [11]. Authors [6] note, that the observed crossover from semiconducting to metallic behavior cannot be explained by thermal activation of the carriers, rather, the granular nanocrystalline CuI structure should be the reason for this behavior. In [1] investigation on the transport mechanism for polycrystalline CuI thin films by studying temperature-dependent resistivity for over ten samples with different carrier concentrations allowed to construct a conclusive barrier model, which is applicable to describe the conductivity in CuI thin films by the presence of a tunneling process, which model was proposed by Sheng [12]. In [12] a theoretical expression for the tunneling conductivity was derived, which displays thermally activated characteristics at high temperatures, but becomes identical to the temperature-independent simple elastic tunneling at low temperatures. Between the two limiting behaviors, the shape of the tunneling barrier controls the temperature dependence of the conductivity.

In accordance with [1, 6], the modeling of the transport properties, when CuI film demonstrates a metallic behavior (for the branch of the resistivity vs. temperature graph where $d\rho/dT > 0$) leads to an insight into the properties of the interior of the CuI grains. A simple power law was used in [1, 6] for the metallic CuI film, which resistivity ρ_m reasonable explanation is the scattering on ionized impurities explicitly derived for degenerate semiconductors, and also carrier–carrier scattering. According to [1], both processes are justified due to the high carrier densities in CuI and produce a similar quadratic temperature dependence of the resistivity:

$$\rho_m(T) = \rho_0 + \rho_{02} T^{\gamma}. \tag{1}$$

Here ρ_0 is a residual offset resistivity at $T = 0$ K, ρ_{02} is a temperature-independent prefactor, and γ is a numerical exponent (according to [1], fitting with $\gamma = 2$ reproduces the data fairly well). Similarly, it states in [6] that within the metallic region, the

conductivity follows the power law, $\sigma_m(T) \sim T^{-2}$, according to the ionized impurity scattering model for degenerate semiconductors.

The semiconducting temperature dependence of the CuI resistivity ρ_s (in the branch of the resistivity vs. temperature graph where $d\rho/dT < 0$) is explained, according to [1, 6], by the granular structure of the CuI films, and a model capable of reproducing the semiconducting behavior of CuI thin films is a fluctuation-induced tunneling conductivity (FITC) model developed by Sheng [12]. According to [12], consider a region of close approach between two large conducting segments in a disordered material. Since the electron tunneling probability depends exponentially on the insulating barrier thickness, it is expected that practically all tunneling occurs within the small surface areas. We can approximate such a tunnel junction by a parallel-plate capacitor. Owing to the random thermal motion of electrons in the conducting region, there can be transient excess or deficit of charges on the tunnel junction surfaces, resulting in voltage fluctuations across the junction. Since the internal tunnel junctions in disordered materials are usually small in area, the resulting large voltage fluctuations across the junctions are expected to play an important role in modifying the electron tunneling probability. As shown in [1, 6, 7], FITC model is applicable for degenerate CuI thin films, when most of the conduction electrons are delocalized and free to move up to several atomic distances inside the crystal grains. Along with this, FITC model assumes energetic barriers between conducting regions of CuI grains, which are overcome by a tunneling process. This process takes place at the point of closest approach between the conducting regions that is, across the grain boundaries. The tunneling current applied for CuI films has an additional temperature dependence due to thermal voltage fluctuations at the barriers, which results in a typical temperature dependence of the conductivity for FITC model described in [1, 6] as follows:

$$\sigma_S(T) = \sigma_1 \exp[-T_0/(T + T_{0S})], \tag{2}$$

where σ_1 is a prefactor that is only weakly temperature-dependent, two temperatures T_0 and T_{0S} have a physical interpretation: T_0 corresponds to the energy needed to overcome the barrier, while well below T_{0S} the thermal voltage fluctuations become insignificant and the resistivity stays almost temperature independent.

As a special case of FITC [1, 6, 12], it is proved in [7] that transport of charge carriers in polycrystalline CuI films evaporated in a vacuum takes place via the localized states, and this transition through localized states is named as hopping. The conduction mechanism at near-room temperatures is nearest neighboring hopping (NNH). In NNH conduction, hole hops the nearest neighboring empty sites according to [7] and the temperature dependence of the resistivity is as follows:

$$\rho_S(T) = \exp(T_0/T), \tag{3}$$

where T_0 is a characteristic temperature (i.e. T_0 is the hopping energy in Kelvin degree). As stated in [7], the condition for NNH is, NNH distance (r) $\gg$Bohr exciton radius, which should be satisfied in polycrystalline CuI films (CuI Bohr exciton

radius is 1.5 nm [13]). Thus, for the branch of the resistivity versus temperature graph where $d\rho/dT < 0$, the slope of the linear fitting of $\ln(\rho_s)$ vs $1/T$ gives hopping energy T_0, which is lesser than the activation energy required for the thermally activated transition of charge carriers to the valence band. The nearest neighboring hopping model fits the resistivity of the thermally evaporated cubic cuprous iodide films at near-room temperatures [7] with $T_0 \approx 38.6$ K, that equals to $T_0 \approx 3.3$ meV.

As it was found from the literature survey, no work has been done on the transport properties of CuI thin films deposited by SILAR, despite the fact that the development and improvement of these materials require thorough knowledge about their electrical and thermoelectric properties. Hence, issues remain to require further experiments to gain a complete picture on hole conductivity in these CuI films and to govern the electronic and transport properties of the CuI films deposited both on rigid and flexible substrates via different SILAR modes. In present work, we investigate an interconnection of crystal structure, morphology, and composition of CuI films produced in different modes of SILAR on glass plates and on flexible poly(ethylene terephthalate) (PET) substrates with their transport properties, and with electrical and thermoelectric properties as a whole.

3.2 Experimental Procedure

In this study, CuI thin films were synthesized via SILAR method both on soda lime glass substrates and on the flexible and transparent 20 μm thick PET films. The deposition of copper iodide films was carried out using an aqueous solution containing 0.1 M $CuSO_4$ and 0.1 M $Na_2S_2O_3$ as a cationic precursor, in which a copper (I) thiosulfate complex $Na[Cu(S_2O_3)]$ was formed, from which Cu^+ ions were released into solution. The glass plate and PET film inserted in a frame "back-to-back" immersed into the cationic precursor for 20 s. Then, the substrates washed in distilled water for 10 s. For the reaction of the firmly adsorbed Cu^+ ions on the glass and PET surfaces with I^- ions to obtain some CuI monolayers, the substrates were then immersed for 20 s into aqueous NaI solution (anionic precursor), which concentration was 0.05, 0.075 or 0.1 M. After that, the glass and PET substrates washed in distilled water for 10 s. The listed procedure was one SILAR cycle of CuI film deposition. Such SILAR cycles were repeated 25–40 times. Thereafter, CuI films deposited on the one side of each substrate, namely CuI/glass and CuI/PET samples, taken out of the frame, washed with distilled water and dried by air stream. As seen in photo of CuI/PET sample in Fig. 3.1a, b, the resulting CuI films are semi-transparent, yellowish in color, and well bonded to the substrates. The thickness of the CuI films in the 100–820 nm range determined gravimetrically, taking for a calculation the bulk CuI density 5.67 g/cm^3.

The morphology of the CuI films observed by scanning electron microscopy (SEM) in secondary electron mode. The SEM instrument (Tescan Vega 3 LMH) operated at an accelerating voltage of 30 kV without the use of additional conductive coatings. Elemental analysis of the CuI films was carried out by X-ray fluorescence

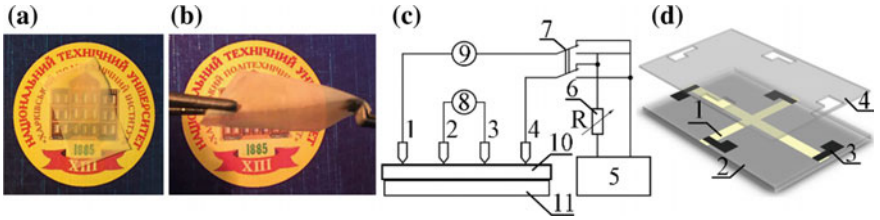

Fig. 3.1 **a**, **b** Two images of 200 nm thick CuI film deposited by SILAR (anionic precursor 0.075 M NaI, 25 SILAR cycles) on PET on the background of National Technical University "Kharkiv Polytechnic Institute" logo. **c** Schematic of apparatus for a studying of CuI film temperature-dependent resistivity using the four-probe method: 1–4—the system of probes; 5—current source; 6—variable resistor for regulating the operating mode of the power supply of the measuring circuit; 7—current direction switch; 8—voltmeter for U_{23} measuring; 9—current I_{14} measuring electrometer; 10—CuI/glass or CuI/PET sample; 11—resistive heater. **d** Schematic of CuI/glass sample for measurement of resistance R of CuI film strip (1) on glass substrate (2) connected with ohmic metal contacts (3), which were deposited by vacuum evaporation of metal through a shadow mask (4) on the surface of CuI

(XRF) microanalysis using an energy dispersive spectrometry (EDS) system "Bruker XFlash 5010". Energy dispersion spectra were taken from the 50 × 50 μm CuI film areas. Quantification of the spectra carried out in the self-calibrating detector mode.

To analyze phase composition and structural parameters of the CuI films, we recorded X-ray diffraction patterns by a "DRON-4" diffractometer as in [10] (XRD method). The microstrains ε in the polycrystalline CuI films $\varepsilon = \Delta d/d$ (where d is the crystal interplanar spacing according to the reference database JCPDS, and Δd is the difference between the corresponding experimental and reference interplanar spacings) were estimated by an analyzing the broadening of the X-ray diffraction peaks using the Scherrer's method [7]. The average crystallite size (D) was calculated using Scherrer's semi-empirical formula [7]:

$$D = (0.9 \cdot \lambda)/(\beta \cdot \cos\theta), \tag{4}$$

where λ is X-ray wavelength; $\beta = (B - b)$, when B is the observed Full Width at Half Maximum (FWHM), and b is the broadening in the peak due to the instrument in radians, θ denotes the Bragg's angle of the X-ray diffraction peak.

The conductivity type of the obtained CuI films determined using a standard hot-probe method.

The resistivity ρ of CuI films in all CuI/glass and CuI/PET samples was measured at temperatures T from 290 to 390 K in accordance with [14] by means four-point collinear probe resistivity method using a home-made apparatus for a studying the temperature-dependent resistivity presented in Fig. 3.1c. The resistivity was calculated according to [14] as follows:

$$\rho = (\pi\, t\, \delta\, U_{23})/(I_{14} \ln(2)), \tag{5}$$

where U_{23} is the voltage between the second and third probe; I_{14} is the current between the first and fourth probes; δ is a correction factor for the accounting the ratio of the distance between the probes and the size of the substrate; $\pi\delta/\ln(2) \approx 4.45$.

Additionally, for some CuI/glass samples, we measured resistivity using resistances R of CuI film strips on glass substrates connected with two opposite ohmic metal contacts. These contacts were deposited by vacuum evaporation of metal through a shadow mask on the surface of CuI as shown in Fig. 3.1d. To study the temperature-dependent resistivity, the CuI/glass sample was heated in the T range 290–345 K using a hot plate of a Peltier element "TEC1-12730", on which it was located. Resistivity value was obtained by the expression:

$$\rho = twRl^{-1}, \tag{6}$$

where t is CuI film thickness, w is *the* width of CuI film strip; R is resistance between two metal contacts, l is the length of CuI film strip.

To assess the thermoelectric performances of the obtained CuI films, the in-plane Seebeck coefficients S at the 295–395 K temperature range were obtained according to [14] as thermoelectric voltages induced in response to the temperature gradients ΔT along the CuI/glass and CuI/PET samples. As shown earlier [14], thermoelectric voltages were measured when a distance between hot and cold probes in the form of gold rings in the home-made setup was 2.3 cm.

3.3 Results and Discussion

Figures 3.2a and 3.3a show the morphology of CuI films prepared on glass and on PET substrates, respectively, by SILAR depending on the anionic precursor concentration. A tiny network like fibrous CuI structure for the SILAR deposited film is shown, especially on the glass substrate, when using as the anionic precursor of the dilute solution 0.05 NaI. The elevated anion precursor concentrations provide an increase in the thickness of copper iodide films and a change in the morphology of their surface. The smoothest dense fine-grained CuI layers were obtained using an aqueous solution of 0.075 mM NaI as the anion precursor, the further increase of the NaI concentration up to 0.1 M resulted in a coarse-grained CuI, especially on the glass substrate.

Figures 3.2b and 3.3b demonstrate experimental XRD pattern for these samples of copper iodide films deposited by SILAR on glass and on PET substrates, respectively. As can be seen, all CuI films are single-phase, polycrystalline and have a cubic Marshite copper iodide structure (zincblende, γ-CuI, JCPDS#06-0246). Calculations of the CuI crystallite sizes (coherent-scattering domains) yielded the 15–50 nm range, so, the films are nanocrystalline. Analysis of structural parameters of the obtained copper iodide films has revealed tensile microstrains $\varepsilon = (2.7–12.0) \times 10^{-3}$ arb. un.

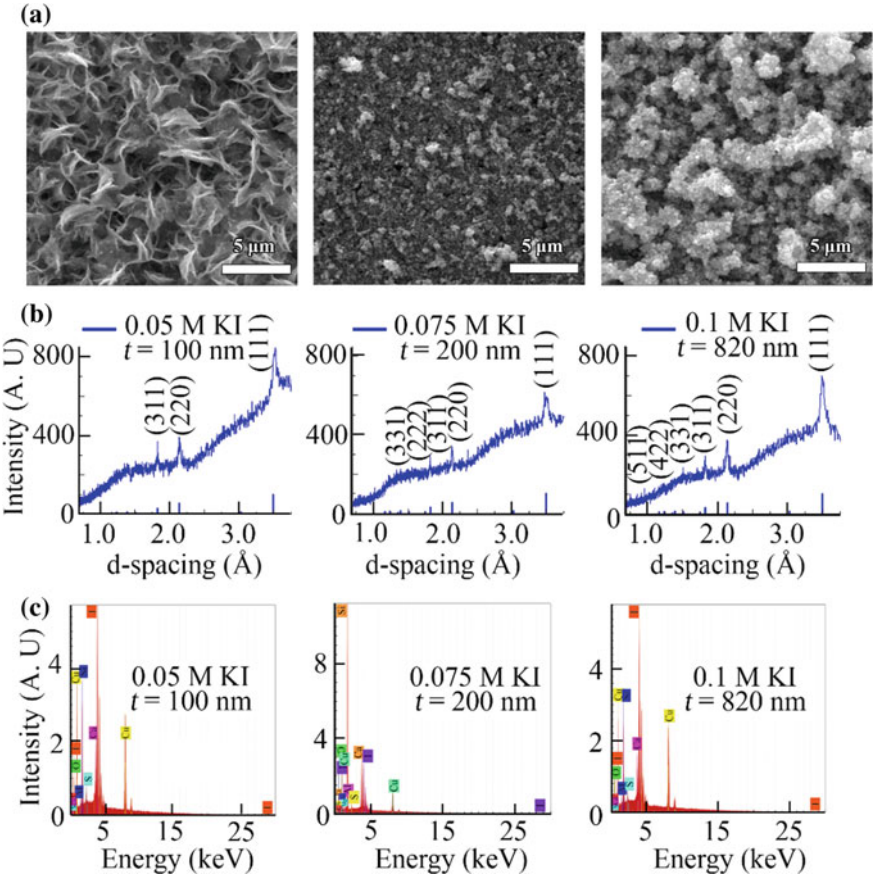

Fig. 3.2 Top-view SEM images of copper iodide films deposited on glass substrates via SILAR using anionic precursors with different NaI concentrations. XRD patterns (**b**) and the corresponding X-ray fluorescence spectra (**c**) of CuI films deposited on glass substrates via SILAR method using anionic precursors with different NaI concentrations

No significant effect of the substrate on the CuI crystal structure was found. CuI/glass and CuI/PET samples deposited by SILAR using 0.075 M NaI have shown the best CuI crystal structure.

The elemental X-ray fluorescence microanalysis of these CuI films (Figs. 3.2c, 3.3c) has revealed, that the elemental ratio (at. %) of the Cu/I is more than one (Cu/I ratio in the 1.2–1.4 range). Some other elements have also been found in the XRF spectra. Among them, it is established that Si, Na, Mg, Ca, O in Fig. 3.2c belong to the glass substrate. C and O belong to the PET Fig. 3.3c or might be attributed for both samples to H_2O, O_2, and CO_2 adsorbed on the surface of the CuI crystals in the air. A small peak of aluminum observed in the energy dispersion spectra is apparently generated by aluminum attachments of the vacuum chamber, in which the XRF

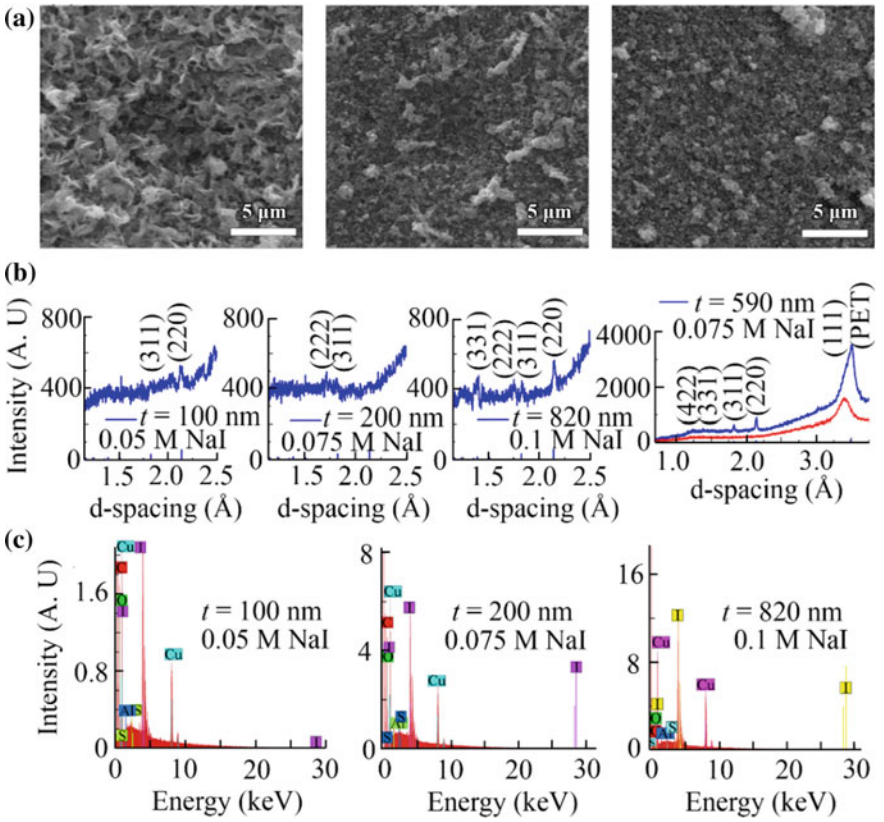

Fig. 3.3 Top-view SEM images of copper iodide films deposited on PETsubstrates via SILAR using anionic precursors with different NaI concentrations. XRD patterns (**b**) and the corresponding X-ray fluorescence spectra (**c**) of CuI films deposited on glass substrates via SILAR method using anionic precursors with different NaI concentrations, and XRD pattern of PET substrate

microanalysis was carried out, primarily, by the table and the holder for the samples. A distinctive feature of all obtained by us via the SILAR technique CuI films is the presence of 0.3–2.0 at.% of sulfur, the source of which, probably, is a chemically unstable compound sodium thiosulfate $Na_2S_2O_3$ from the cationic precursor solution. Despite the fact, that we could not find such information in the literature, to our opinion, sulfur, which is an element of the sixth group, can form acceptor levels in the copper iodide. Thus, sulfur can increase the number of free charge carriers (holes) in the *p*-CuI films making them degenerate semiconductors without formation of a distinguishable via X-ray diffractometry analysis copper sulfide phases.

The conventional hot probe method has identified that all obtained by means SILAR CuI films are *p*-type semiconductors. Comparison of Figs. 3.4, 3.5 and 3.6 shows that, in general, the resistivity of CuI films is low, but ρ for CuI/glass samples is greater than for CuI/PET ones. For our CuI/glass samples, ρ is in the range of

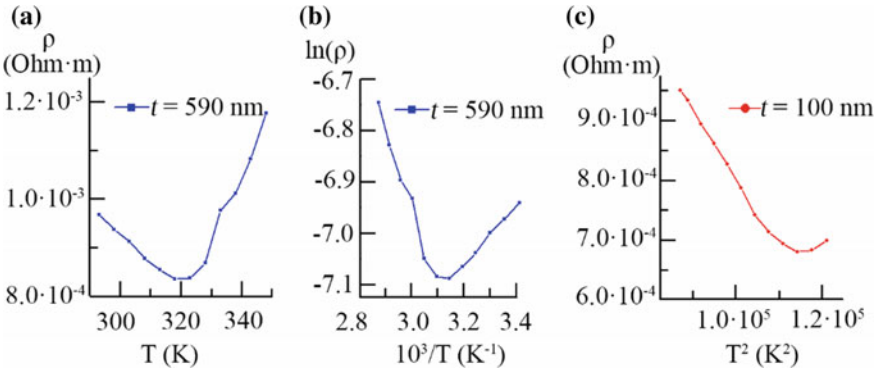

Fig. 3.4 Temperature dependences of resistivity ρ for CuI/glass samples in the form of 100 nm and 590 nm thick CuI strips connected with metal contacts on glass substrates: **a** resistivity versus temperature graphs; **b** ln ρ versus 1000/T graphs; **c** ρ versus T^2 graphs

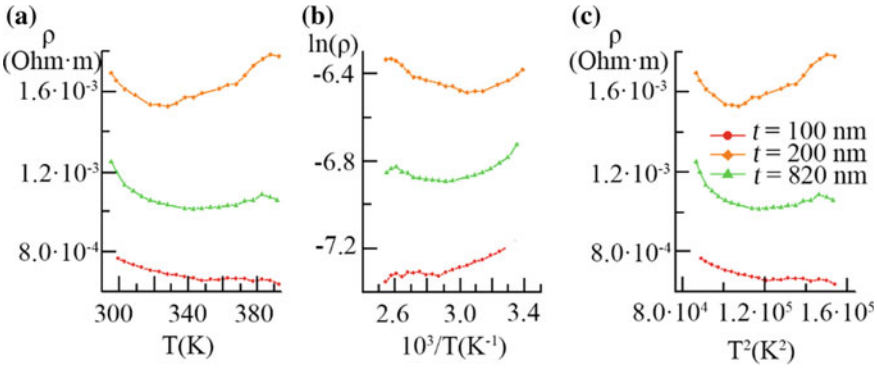

Fig. 3.5 Temperature dependences of resistivity ρ measured by means four-point probe method for CuI/glass samples with 100 nm, 200 nm and 890 nm thick CuI films: **a** resistivity versus temperature graphs; **b** ln ρ versus 1000/T graphs; **c** ρ versus T^2 graphs

6.8×10^{-4}–1.8×10^{-3} Ω m at 290–390 K. The CuI/PET samples have ρ in the 3.0×10^{-4}–1.0×10^{-3} Ω m range in the T interval 290–380 K.

The results of the transport properties analysis of the cubic cuprous iodide films are presented in Figs. 3.4, 3.5 and 3.6. It is seen that the substrate material affects the character of CuI resistivity changes with temperature to a certain extent, but only for the thinnest CuI films. With increasing of the CuI film thickness in both CuI/glass and CuI/PET samples, the effect of the substrate on the transport of carriers decreases, as can be seen in Figs. 3.4, 3.5 and 3.6. This is explained by the layer-by-layer growth of the films in the SILAR method. For 200–820 nm thick CuI films the crossover is observed from ρ decreasing with T increasing to ρ growth with T. The first behavior (semiconducting) is more characteristic for CuI/glass samples (Figs. 3.4, 3.5), and the second trend (metallic) dominates for CuI/PET samples (Fig. 3.6). Thin 100 nm

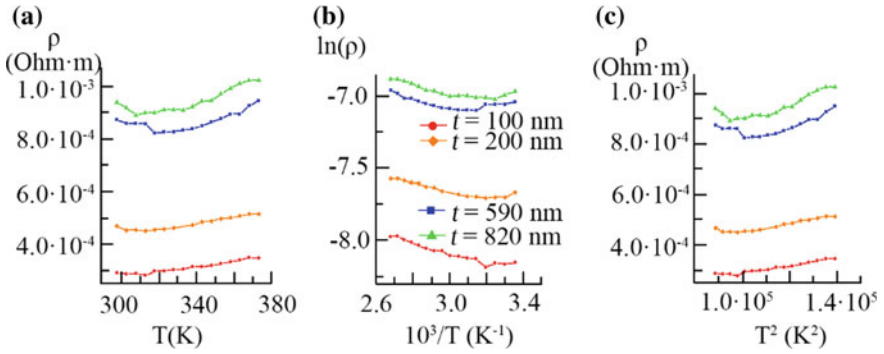

Fig. 3.6 Temperature dependences of resistivity ρ measured by means four-point probe method for CuI/PET samples with 100, 200, 590 and 890 nm thick CuI films: **a** resistivity versus temperature graphs; **b** ln ρ versus 1000/T graphs; **c** ρ versus T^2 graphs

CuI films in CuI/glass samples prepared by SILAR using diluted anionic precursor 0.05 M NaI demonstrate only semiconductor behavior at the T range 290–340 K (Figs. 3.4, 3.5). It is significant that the values of CuI resistivity and their changes with temperature are almost the same for CuI/glass samples regardless of the method of ρ measurement, i.e. for the approach using CuI strips connected by ohmic contacts (Fig. 3.4), and for a four-probe method (Fig. 3.5). On the contrary, the 100 nm CuI film obtained in the identical mode of SILAR on PET exhibits only metallic properties in the temperature range from 300 to 380 K (Fig. 3.6).

As it is seen from ln ρ versus 1000/T plots for most samples in Figs. 3.4b, 3.5, and 3.6b, at T near 290 K the temperature dependence of the resistivity fits carrier transport through nearest neighboring hopping [7] with hopping energy T_0 in the 10–76 meV range (Table 3.1).

Simultaneously, at T near 380–390 K most CuI films demonstrate metallic transport (Figs. 3.4, 3.5 and 3.6). It is seen from ρ versus T^2 plots in Figs. 3.4c, 3.5 and 3.6c, for all CuI/PET samples, and also for CuI/glass samples with 200–820 nm thick CuI films. Their resistivity follows the power law, $\rho_m(T) \sim T^2$ according to the ionized impurity scattering and carrier–carrier scattering model for degenerate semiconductors [1, 6].

The larger ρ_{02} values have revealed the more intense scattering on ionized impurities and carrier–carrier scattering for CuI/glass samples as compared with CuI/PET samples (Table 3.1) at T near 380–390 K. At the same time, the hole transport at T near 290 K is limited by barriers at the grain boundaries in the CuI/glass samples to a greater extent, since they have more height barriers (T_0 in the 27–76 meV range) compared to CuI/PET samples (T_0 in the 10–42 meV range).

As seen in Figs. 3.2 and 3.3, the observed transport properties of CuI films correspond to their nanocrystalline structure and nanostructured surfaces. However, it is impossible to explain the difference in transport properties of CuI/glass and CuI/PET samples, based only on our data on the morphology of the surfaces, the crystal structure and the composition of the CuI films. At the same time, the data on thermal

Table 3.1 Transport properties and Seebeck coefficients of CuI films produced by the different modes of SILAR method on glass and PET substrates

SILAR mode	CuI film carrier transport parameters and Seebeck coefficient							
Cationic precursor	Anionic precursor	Thickness t, nm	PET substrate	Glass substrate				
			ρ_{02}, ΩmK^{-2}	T_0, meV	S, μV/K	ρ_{02}, ΩmK^{-2}	T_0, meV	S, μV/K
0.1 M $CuSO_4$, 0.1 M $Na_2S_2O_3$	0.05 M NaI	100	2×10^{-9}	15	115	3×10^{-9} C	71 C	207
						–	27	
	0.075 M NaI	200	3×10^{-9}	10	85	6×10^{-9}	33	188
		590	2×10^{-9}	20	123	2×10^{-8} C	49 C	251
	0.1 M NaI	820	4×10^{-9}	42	113	2×10^{-9}	76	179

C—CuI strips connected with metal contacts on glass substrates

electromotive forces (Seebeck coefficients) given in Table 3.1 demonstrate the lower *S* values for all CuI/PET samples compared to CuI/glass samples, which is well correlated with their transport properties, as the Seebeck coefficient is a property, which depends on the electronic structure near the Fermi-level of degenerate semiconductors. According to [15], the *S* decreasing in CuI/PET samples is explained due to the fact, that these degenerate semiconducting CuI films behave more like metals than semiconductors.

3.4 Conclusions

The paper demonstrates the transport properties of nanocrystalline cubic cuprous iodide films deposited by SILAR on glass and PET substrates. Temperature dependences of resistivity for most CuI films in CuI/glass and CuI/PET samples have the crossover from semiconducting to metallic behavior with *T* increasing, which is typical for degenerate semiconductors. It has been confirmed that the semiconductor carrier transport occurs at *T* near 290 K through the nearest neighboring hopping. Metallic transport in CuI films carried out at *T* near 380–390 K in accordance with the ionized impurity scattering and the carrier–carrier scattering model for degenerate

semiconductors. Comparison of thermoelectric properties is yet another confirmation of the fact that the degree of degeneration of CuI semiconductors in CuI/PET samples is higher than in CuI/glass samples deposited by SILAR method.

References

1. M. Kneiß, C. Yang, J. Barzola-Quiquia, G. Benndorf, H. von Wenckstern, P. Esquinazi, M. Lorenz, M. Grundmann, Suppression of grain boundary scattering in multifunctional p-type transparent γ-CuI thin films due to interface tunneling currents. Adv. Mater. Interfaces **5**(6), 1701411-1 (2018)
2. M. Grundmann, F.-L. Schein, M. Lorenz, T. Böntgen, J. Lenzner, H. Wenckstern, Cuprous iodide—a p-type transparent semiconductor: history and novel applications. Phys. Status Solidi A **210**, 1671 (2013)
3. N. Yamada, R. Ino, Y. Ninomiya, Truly transparent p-type γ-CuI thin films with high hole mobility. Chem. Mater. **28**(14), 4971 (2016)
4. F.-L. Schein, H. von Wenckstern, M. Grundmann, Transparent p-CuI/n-ZnO heterojunction diodes. Appl. Phys. Lett. **102**, 092109-1 (2013)
5. S. Inudo, M. Miyake, T. Hirato, Electrical properties of CuI films prepared by spin coating. Phys. Status Solidi A **210**(11), 2395 (2013)
6. C. Yang, M. Kneiβ, M. Lorenz, M. Grundmann, in *Proceedings of the National Academy of Sciences of the United States of America*, ed. by A. Rockett (USA, 2016)
7. D.K. Kaushik, M. Selvaraj, S. Ramu, A. Subrahmanyam, Thermal evaporated copper iodide (CuI) thin films: a note on the disorder evaluated through the temperature dependent electrical properties. Sol. Energ. Mat. Sol. C **165**, 52 (2017)
8. A. Pishtshev, S.Z. Karazhanov, Structure-property relationships in cubic cuprous iodide: a novel view on stability, chemical bonding, and electronic properties. J. Chem. Phys. **146**(6), 064706-1 (2017)
9. N.P. Klochko, V.R. Kopach, G.S. Khrypunov, V.E. Korsun, N.D. Volkova, V.N. Lyubov, M.V. Kirichenko, A.V. Kopach, D.O. Zhadan, A.N. Otchenashko, n-ZnO/p-CuI barrier heterostructure based on zinc-oxide nanoarrays formed by pulsed electrodeposition and SILAR copper-iodide films. Semiconductors **51**, 789 (2017)
10. N.P. Klochko, K.S. Klepikova, V.R. Kopach, I.I. Tyukhov, D.O. Zhadan, G.S. Khrypunov, S.I. Petrushenko, S.V. Dukarov, V.M. Lyubov, M.V. Kirichenko, A.L. Khrypunova, Semitransparent p-CuI and n-ZnO thin films prepared by low temperature solution growth for thermoelectric conversion of near-infrared solar light. Sol. Energy **171**, 704 (2018)
11. N.P. Klochko, V. Kopach, G. Khrypunov, V. Korsun, V. Lyubov, O. Otchenashko, D. Zhadan, M. Kirichenko, V. Nikitin, M. Maslak, A. Khrypunova, in *Proceedings of the 2017 IEEE 7th International Conference on Nanomaterials: Applications and Properties (NAP)*, Odessa, Ukraine, 2017, Part 2 (IEEE, 2017), p. 02NTF01
12. P. Sheng, Fluctuation-induced tunneling conduction in disordered materials. Phys. Rev. B **21**(6), 2180 (1980)
13. Y. Yang, S. Liu, K. Kimura, Synthesis of well-dispersed CuI nanoparticles from an available solution precursor. Chem. Lett. **34**(8), 1158 (2005)
14. N.P. Klochko, V.R. Kopach, I.I. Tyukhov, G.S. Khrypunov, V.E. Korsun, V.O. Nikitin, V.M. Lyubov, M.V. Kirichenko, O.N. Otchenashko, D.O. Zhadan, M.O. Maslak, A.L. Khrypunova, Wet chemical synthesis of nanostructured semiconductor layers for thin-film solar thermoelectric generator. Sol. Energy **157**, 657 (2017)
15. A. Shakouri, Recent developments in semiconductor thermoelectric physics and materials. Annu. Rev. Mater. Res. **41**(1), 399 (2011)